

Fission dynamics at low excitation energy

Y. Aritomo¹, S. Chiba¹ and F. Ivanyuk^{1,2}

¹ *Research Laboratory for Nuclear Reactors, Tokyo Institute of Technology, Ookayama, Meguro-ku, Tokyo, 152-8850, Japan and*

² *Institute for Nuclear Research, Kiev, Ukraine*

The mass asymmetry in the fission of ^{236}U at low excitation energy is clarified by the analysis of the trajectories obtained by solving the Langevin equations for the shape degrees of freedom. It is demonstrated that the position of the peaks in the mass distribution of fission fragments is determined mainly by the saddle point configuration originating from the shell correction energy. The width of the peaks, on the other hand, results from the shape fluctuations close to the scission point caused by the random force in the Langevin equation. We have found out that the fluctuations between elongated and compact shapes are essential for the fission process. According to our results the fission does not occur with continuous stretching in the prolate direction, similarly to that observed in starch syrup, but is accompanied by the fluctuations between elongated and compact shapes. This picture presents a new viewpoint of fission dynamics and the splitting mechanism.

PACS numbers: 25.70.Jj, 25.85.w, 27.90.+b, 28.41.-i

Keywords: fission process, two-center shell model, Langevin equations, dynamical trajectories, mass distribution and total kinetic energy of fission fragments

I. INTRODUCTION

Since the discovery of fission of uranium in 1938 [1, 2], the principle of this phenomenon has been studied owing to its scientific interest. The application of fission process to the supply of power was realized soon after its discovery. However, the mass-asymmetric fission remained a puzzle as far as nuclei were described in the analogy with the liquid drop [3]. The origin of the asymmetry in the mass distribution of fission fragments (MDFFs) nowadays is related to the shell structure of the fissioning nucleus. Many theoretical dynamical models have been applied to nuclear fission at low excitations in an attempt to explain its mechanism [4–9].

In order to investigate the time evolution of the nuclear shape during the fission process a dynamical approach using the Langevin equation can be used. In our previous study [10] this approach was applied to the fission of $^{234,236}\text{U}$ and ^{240}Pu at low excitation energies with account of the shell structure of these nuclei. In these calculations we obtained an asymmetric MDFF and the total kinetic energy (TKE) of the fission fragments that agreed well with the experimental data.

In the present work, we attempt to clarify the origin of the asymmetric MDFF of ^{236}U at a low excitation energy by the analysis of the time evolution of nuclear shape and trajectories calculated within the Langevin approach. We have found the factors determining the positions and widths of the peaks in the MDFF: the former is mainly related to the positions of the fission saddle, which is influenced by the shell correction energy, and the latter is related to the thermal fluctuation caused by the random force in the Langevin equation close to the scission point.

In addition, we observed a new phenomenon in the mechanism of fission dynamics: the fluctuation of the shape of fissioning nucleus between the compact and elon-

gated configurations on the way to the scission point. By comparing the TKE of the fission fragments obtained experimentally and by our calculation, we confirmed that such a configuration is realized there. This leads to the picture in which the fission does not occur in the manner of starch syrup, which grows with continuous stretching until the neck radius gets very small.

Below we present the arguments in favor of this new interpretation of fission dynamics at low excitation energy. The paper is organized as follows. In Sec. II, we describe in detail the framework of the model. In Sec. III, we discuss the potential energy landscape and reveal the effect of the shell structure on the mass-asymmetric fission of ^{236}U at $E^* = 20$ MeV by analyzing the dynamical trajectories. In Sec. IV, we investigate the configuration at the scission point. In Sec. V, the TKE of the fission fragments is discussed. A short summary of this study and further discussion are presented in Sec. VI.

II. THE MODEL

We use the fluctuation-dissipation model and employ the Langevin equations [11] to investigate the dynamics of the fission process. The nuclear mean field is defined by the two-center shell model potential [12, 13] which includes the central part, \mathbf{I}_1 and \mathbf{I}_2^2 terms. The central part consists of two oscillator potentials smoothly joined by the fourth order polynomial. Within the two-center shell-model parameterization (TCSMP) the shape is characterized by 5 deformation parameters: the distance z_0 between the centers of left and right oscillator potentials, the deformations δ_1 and δ_2 of the left and right oscillator potentials, the neck parameter ϵ and the mass asymmetry $\alpha = (A_1 - A_2)/(A_1 + A_2)$, where A_1 and A_2 denote the mass numbers of heavy and light fragments [11] (in case of the shape separated into two fragments)

or the masses of the right and left parts of the compact nucleus. Please, note, that within TCSMP the shape is divided in parts by the point $z = 0$.

The formal definition of these parameters is given in Appendix and demonstrated in Fig. 9.

In order to reduce the computation time we use in this work the restricted deformation space. We assume that the parameters δ_1 and δ_2 are the same, $\delta_1 = \delta_2 = \delta$. The parameters δ_1 and δ_2 fix the deformation of *potential* in "outer" region, namely for $z \leq z_1$ or $z_2 \leq z$, see Fig. 9. The deformation of *fragments* depends not only on δ_1 and δ_2 but on all other parameters, z_0 , ϵ and α . Changing elongation or mass asymmetry one can get the fragments with different deformation even if δ_1 is put equal to δ_2 .

The neck parameter ϵ is kept fixed. Here, like in the previous works, we use the value $\epsilon = 0.35$, which was recommended in Ref. [14] for the fission process. Keeping ϵ fixed does not mean that the neck radius is fixed. It is clearly demonstrated by Fig. 9 in the Appendix. The neck radius in TCSMP depends on all deformation parameters. When we change the elongation, mass asymmetry or deformation of fragments the neck radius changes too.

Thus, with three deformation parameters z_0 , α and δ we take into account the three most important degrees of freedom for the fission process: elongation, mass asymmetry and the neck radius.

For the sake of convenience, like in previous works, instead of z_0 we employ the scaled coordinate \bar{z}_0 defined as $\bar{z}_0 = z_0/(R_{CN}B)$, where R_{CN} denotes the radius of a spherical compound nucleus and B is defined as: $B = (3 + \delta)/(3 - 2\delta)$. The three deformation parameters \bar{z}_0 , α and δ are considered as the dynamical variables.

These three collective coordinates may be abbreviated as q , with $q = \{\bar{z}_0, \alpha, \delta\}$. For a given value of the intrinsic excitation energy characterized by the temperature T the potential energy is defined as the sum of the liquid-drop (LD) part and the microscopic (SH) part,

$$\begin{aligned} V(q, T) &= V_{LD}(q) + V_{SH}(q, T), \\ V_{LD}(q) &= E_S(q) + E_C(q), \\ V_{SH}(q, T) &= [\Delta E_{shell}(q) + \Delta E_{pair}(q)]\Phi(T), \\ \Phi(T) &= \exp(-\bar{a}T^2/E_d). \end{aligned} \quad (1)$$

In (1) the V_{LD} is the potential energy calculated with the finite-range liquid drop model [15], given by the sum of the surface energy E_S and the Coulomb energy E_C . The microscopic energy V_{SH} at $T = 0$ is calculated as the sum of the shell correction energy ΔE_{shell} and the pairing correlation correction energy ΔE_{pair} . We assume that the angular momentum of fissioning nucleus at the low excitation energy is not large, so the rotational energy is not included in (1).

The ΔE_{shell} is calculated by Strutinsky method [16, 17] from the single-particle levels of the two-center shell model potential [12, 18, 19] as the difference between the sum of single-particle energies of occupied states and the averaged quantity.

The E_{pair} was evaluated in BCS approximation following [17, 20]. The averaged part of the pairing correlation energy was calculated assuming that the density of single-particle states is constant over the pairing window. The pairing strength constant was related to the average gap parameter $\tilde{\Delta}$ by solving the gap equation in the same approximation and adopting for $\tilde{\Delta}$ the value $\tilde{\Delta} = 12/\sqrt{A}$ suggested in [20] by considering the empirical results for the odd-even mass difference.

The E_d in (1) is the damping parameter of the shell correction chosen to be equal to 20 MeV like in [21]. In the level density parameter [22] both the shell effects [21, 23] and the dependence of average part \tilde{a} on the deformation were taken into account,

$$\begin{aligned} \bar{a} &= \left\{ 1 + \frac{V_{SH}(T=0)}{E_{int}} \left[1 - \exp\left(-\frac{E_{int}}{E_d}\right) \right] \right\} \tilde{a}(q), \\ \tilde{a}(q) &= a_1 A + a_2 A^{2/3} B_s(q), \end{aligned} \quad (2)$$

with A being the mass number of fissioning nucleus and B_s - the reduced surface energy, see [24]. The E_{int} in (2) is the intrinsic excitation energy, see (6) below, calculated at each step of integration of equations of motion.

To calculate the potential energy, we employed the macroscopic-microscopic method and TWOCTR code of the two-center shell model [18, 19, 25]. In this code, the parameters of the finite-range liquid drop model [15] are used $r_0 = 1.20$ fm, $a = 0.65$ fm, $a_s = 21.836$ MeV and $\kappa_s = 3.48$, where r_0 and a are the nuclear-radius constant and the range of the Yukawa folding function, a_s and κ_s are the surface energy constant and the surface-asymmetry constant, respectively. The potential energy V_{LD} and $V_{LD} + V_{SH}$ (denoted by the dash and solid lines, respectively) for ^{236}U with $\delta = 0$, $\alpha = 0$ and $\epsilon = 0.35$, calculated by TWOCTR is presented in Fig. 1.

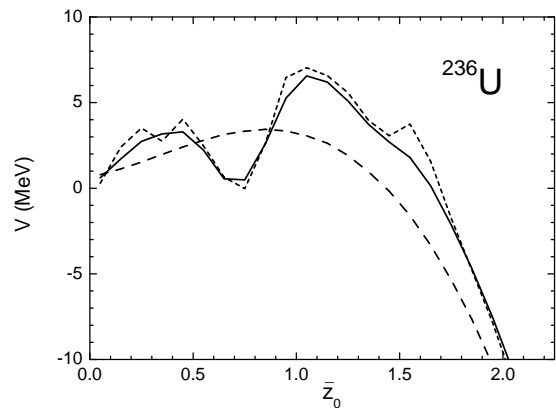


FIG. 1: Deformation dependence of the potential energy of ^{236}U at $T = 0$ calculated by TWOCTR with fixed $\delta = 0$, $\alpha = 0$ and $\epsilon = 0.35$. The V_{LD} and $V_{LD} + V_{SH}$ are denoted by the dash and solid lines, respectively. The short-dash line shows the $V_{LD} + \Delta E_{shell}$.

We assume that the temperature dependence of the microscopic energy V_{SH} is expressed by the factor $\Phi(T)$

in Eq.(1). This dependence was suggested a long ago [6] and was confirmed by many years of experience. We are aware that temperature dependence of ΔE_{shell} and ΔE_{pair} is not the same, see also [26, 27]. Within the BCS approximation the pairing correlations disappear above critical temperature $T_{crit} \approx 0.5 \div 0.6$ MeV while the ΔE_{shell} becomes negligible small at $T \approx 2$ MeV. In present calculations at $E^* = 20$ MeV in most cases the local temperature is larger than the T_{crit} . However, even at $T = 0$ the ΔE_{pair} is small compared with ΔE_{shell} , see Fig. 1 (the short-dash line shows the $V_{LD} + \Delta E_{shell}$). So, the use of approximation (1) should not lead to a large inaccuracy of calculated results.

In our previous study [10], we discussed the temperature dependence of the shell correction energy and the effect of this dependence on the fission process and the MDFP for ^{236}U at $E^* = 20$ MeV. Using the several values of the shell damping energy, we investigated the affection of the MDFP. We have found out that the gross features of MDFP did not change so much in this system.

The multidimensional Langevin equations [11] are given as

$$\begin{aligned} \frac{dq_i}{dt} &= (m^{-1})_{ij} p_j, \\ \frac{dp_i}{dt} &= K_i - \frac{1}{2} \frac{\partial}{\partial q_i} (m^{-1})_{jk} p_j p_k - \gamma_{ij} (m^{-1})_{jk} p_k \\ &\quad + g_{ij} R_j(t), \end{aligned} \quad (3)$$

where $q_i = \{\bar{z}_0, \delta, \alpha\}$ and $p_i = m_{ij} dq_j/dt$ is a momentum conjugate to coordinate q_i . The summation is performed over repeated indices. The conservative force in (3) is represented by the derivative of free energy with respect to deformation, $K_i \equiv -\partial F/\partial q_i$, with $F(q, T) = V(q, T) - \bar{\alpha}T^2$.

The m_{ij} and γ_{ij} in (3) are the shape-dependent collective inertia and the friction tensors, respectively. The wall-and-window one-body dissipation [28–30] is adopted for the friction tensor which can describe the pre-scission neutron multiplicities and total kinetic energy of fragments simultaneously [31]. A hydrodynamical inertia tensor with the Werner-Wheeler approximation for the velocity field [32] was used here.

The normalized random force $R_i(t)$ is assumed to be that of white noise, *i.e.*,

$$\langle R_i(t) \rangle = 0, \quad \langle R_i(t_1) R_j(t_2) \rangle = 2\delta_{ij} \delta(t_1 - t_2). \quad (4)$$

The strength of the random force g_{ij} is related to the friction tensor γ_{ij} by the classical Einstein relation,

$$\sum_k g_{ik} g_{jk} = \gamma_{ij} T. \quad (5)$$

In principle, the inertia and friction tensors may contain the shell effects too. To account for these effects one could consider the microscopic transport coefficients calculated, for example, within the linear response theory and local harmonic approximation [33–35]. It turns out

that friction tensor calculated by the microscopic model is temperature dependent and much smaller than that calculated by the macroscopic model at low temperature. As it follows from the present calculations, the MDFP does not depend much on the magnitude of the friction tensor [10]. So, in present work we use the macroscopic friction and inertia tensors. The investigation of the role of shell effects in the collective inertia and friction coefficients will be the subject of future work.

The temperature T is related to the intrinsic excitation energy of the composite system as $E_{int} = \bar{\alpha}T^2$, where E_{int} is calculated at each step of a trajectory calculation as

$$E_{int} = E^* - \frac{1}{2} (m^{-1})_{ij} p_i p_j - V(q, T = 0). \quad (6)$$

The excitation energy of compound nucleus E^* is given by $E^* = E_{cm} - Q$, where Q denotes the Q -value of the reaction.

The calculation starts from the ground state, which is located at $\bar{z}_0 = 0.0, \delta = 0.2, \alpha = 0.0$. For the initial distribution of collective velocities we assume that at the initial moment the collective kinetic energy of the system is zero. Very soon after the start of calculation the state of the system becomes close to the statistical equilibrium. Such initial conditions are very close to that used in earlier dynamical calculations [36].

The fission events are determined in our calculations by classification of different trajectories in the deformation space. Fission from a compound nucleus is defined as the case that a trajectory overcomes the scission point on the potential energy surface. The scission point is assumed here to be given by the configuration with zero neck radius.

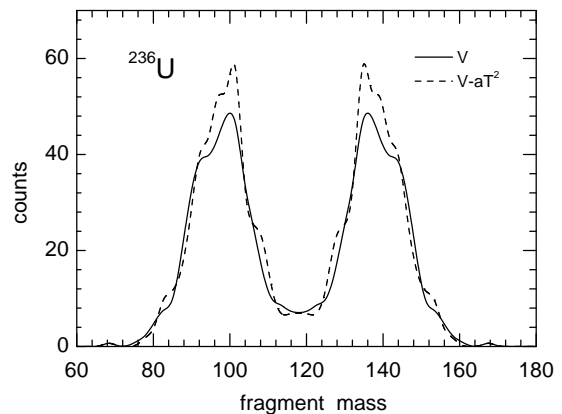


FIG. 2: The comparison of the mass distribution of fission fragments calculated with (dash line) and without (solid line) account of $\bar{\alpha}T^2$ term in (3).

In Fig. 2 we demonstrate the role of $\bar{\alpha}T^2$ in the potential energy in Langevin equations (3). As it is seen from the figure the use of the energy instead of free energy in (3) does not influence much the MDFP of ^{236}U at $E^* = 20$ MeV. So, in all calculations reported below the

term $\bar{a}T^2$ in the potential energy in Langevin equations (3) was neglected.

III. THE ORIGIN OF THE MASS ASYMMETRIC FISSION

In our previous study [10], we investigated the fission of ^{236}U at the excitation energy $E^* = 20$ MeV and have calculated the MDFF, which turned out to agree rather well with experimental data showing that the mass-asymmetric component of the distribution of fission fragments is dominant. In the present paper we try to clarify the origin of the mass-asymmetric fission events of ^{236}U at low excitation energy by analyzing the dynamical trajectories in our model.

To understand the behavior of trajectories and their contribution to the MDFF, we first consider the simple case when the shell effects are neglected and only the liquid drop energy V_{LD} contributes to the potential energy surface (PES).

Fig. 3 shows the trajectories calculated with and without account of random force. To demonstrate the relation to the potential energy the trajectories are placed on the potential energy surface V_{LD} projected onto the \bar{z}_0 - α plane (top) and onto the \bar{z}_0 - δ plane (bottom).

The trajectories calculated without account of random force (heavy solid blue line) start at the saddle point deformation and move down to the separation region along the potential slope due to the drift force $-\partial F/\partial q_i$ in Eq. (3). However, the trajectory does not move along the line of steepest descent. This is a dynamical effect due to the coupling between \bar{z}_0 - and δ -degrees of freedom and the fact that the $\bar{z}_0\bar{z}_0$ - and $\delta\delta$ -components of mass tensor are very different. When the nondiagonal components of mass tensor are neglected (dash red line) the trajectory moves, indeed, along the line of steepest descent, see bottom part of Fig. 3.

In case that the random force is taken into account, the trajectories (thin solid white lines) show the oscillations in the direction of -45° on the \bar{z}_0 - δ plane.

We have analyzed the reason for this special direction and found out that it originates from the properties of the friction tensor, mainly the nondiagonal terms, via the Einstein relation. The detailed explanation will be given separately in a forthcoming paper.

Fig. 4 shows the sample trajectories to the mass-asymmetric fission region calculated with account both of shell effects and random force, placed on the potential energy surface $V_{\text{LD}} + E_{\text{shell}}^0$ and projected onto the \bar{z}_0 - α plane (top) and \bar{z}_0 - δ plane (bottom). Similarly to the calculation in reference [10], the trajectories start at $\{\bar{z}_0, \delta, \alpha\} = \{0.0, 0.2, 0.0\}$, which corresponds to the ground state of the potential energy surface. One can see, that trajectories remain at the ground state (the first minimum) and the second pocket for quite a long time. They even reach large \bar{z}_0 values of $\bar{z}_0 = 1.5 - 1.75$. However, they do not move along straight line to the sep-

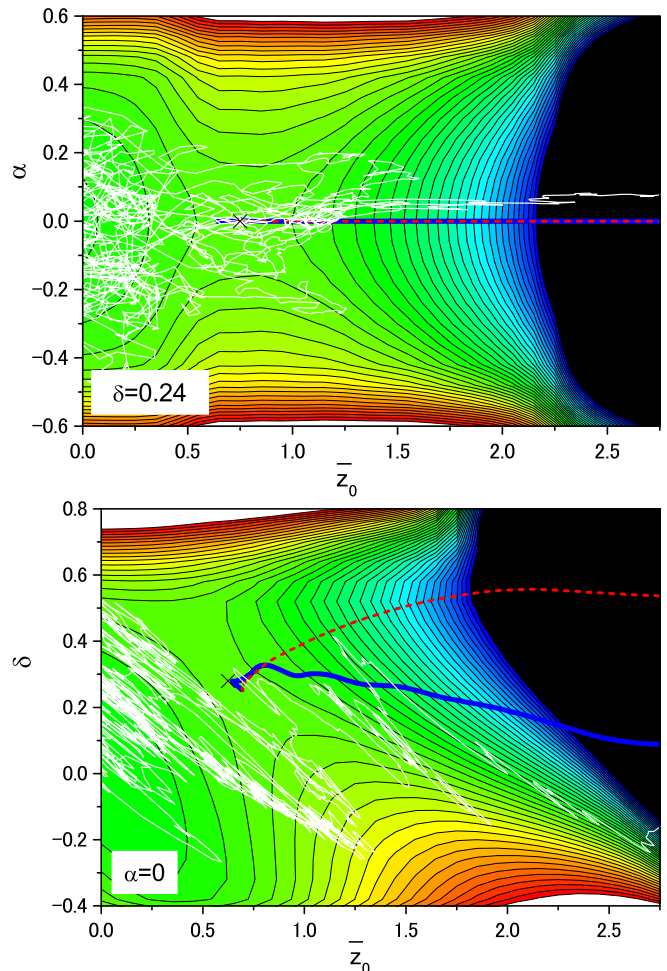


FIG. 3: The examples of trajectories of the fission process of ^{236}U at $E^* = 20$ MeV projected onto the \bar{z}_0 - α plane of V_{LD} $\delta = 0.24$ (top) and on the \bar{z}_0 - δ plane of V_{LD} at $\alpha = 0$ (bottom). The trajectories calculated without random force start at the saddle point.

aration region on the mass-symmetric fission path. Instead, the trajectories pass through the saddle points before moving to the scission region. It is seen that the trajectories leading to mass-asymmetric fission escape from the region around $\{\bar{z}_0, \alpha\} \sim \{0.8, \pm 0.2\}$. In Fig. 4, the fission saddle points are indicated by the symbol \times .

It is seen that the mass-asymmetric fission originates from the trajectories that overcome the fission saddle points located at the mass asymmetry corresponding to the position of the peak of the MDFF, where $A \sim 140$. One can note also that the trajectory on the z - δ plane fluctuates in the direction of -45° , as shown in Figs. 3 and 4. Even after overcoming the fission saddle point, such oscillations are observed up to the scission point.

The reason of these fluctuations may be understood in a following way.

We know from the analysis in [37] that the mass distribution of fission fragments of ^{236}U can be described in terms of *three* fission modes. Two of them are

mass-asymmetric, the so called standard and super-short modes. They differ by the elongation of the shape in the scission region. In principle, there should be two mass-asymmetric valleys in the potential energy surface shown in the bottom part of Fig. 4. In principle, by fluctuations the system can jump from one valley to other. We do not see the two valleys in PES, but the landscape of potential energy is very flat in the direction smaller elongation \leftrightarrow larger elongation (-45°). Within TCSM smaller elongation \leftrightarrow larger elongation corresponds to positive $\delta \leftrightarrow$ negative δ , please, see the demonstration in Fig. 5.

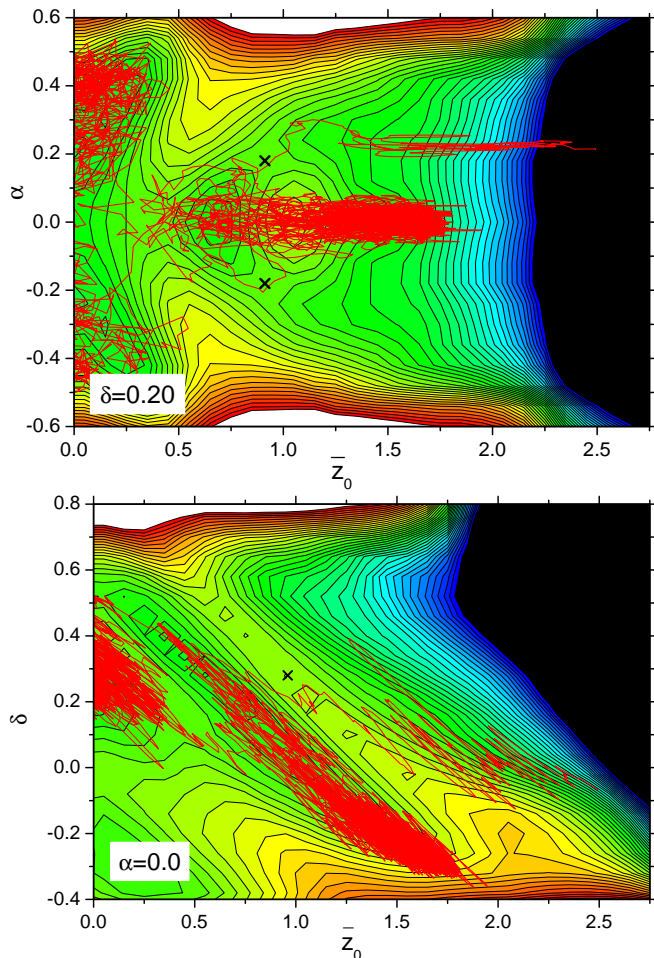


FIG. 4: Sample trajectory projected onto the \bar{z}_0 - α plane at $\delta = 0.2$ (top) and the \bar{z}_0 - δ plane $\alpha = 0.0$ (bottom) of $V_{LD} + E_{\text{shell}}^0$ with $\epsilon = 0.35$ for ^{236}U . The trajectory starts at the ground state $\{\bar{z}_0, \delta, \alpha\} = \{0.0, 0.2, 0.0\}$ at $E^* = 20$ MeV. The fission saddle points are indicated by the symbol \times . The scission lines are denoted by the white lines

If the potential PES is flat even small random force can cause the shape fluctuations of large amplitude. Something like this is observed in present calculations.

So, we would interpret the fluctuations on the way to the scission point observed in our calculations as the transitions between compact and elongated shapes, that both contribute to the mass distributions and TKE.

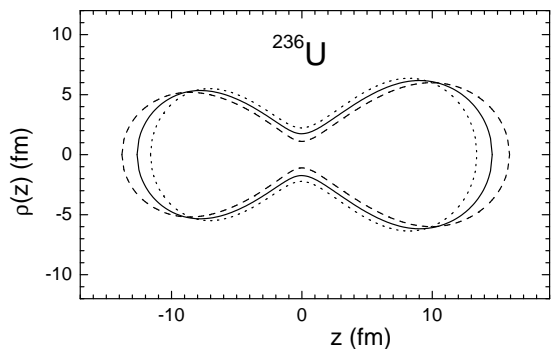


FIG. 5: Nuclear shapes around the scission point of ^{236}U . The dot, solid and dash line corresponds to the nuclear shape at $\{\bar{z}_0, \delta, \alpha\} = \{2.5, -0.2, 0.2\}$, $\{2.5, 0, 0.2\}$ and $\{2.5, 0.2, 0.2\}$.

IV. THE WIDTH OF PEAK IN MDF

The oscillations of the trajectories is a very important feature of the fission dynamics. After overcoming the fission saddle point, as shown in Fig. 4, the trajectories fluctuate frequently and move down the potential slope step by step. The direction of the oscillation is neither parallel nor perpendicular to the contour lines of the potential energy surface. The trajectories climb and descend the potential slope in the result of the random force and drift force, respectively. Correspondingly, the nuclear shape fluctuates around some average value as demonstrated in Fig. 5. The edges of nuclear shape with $\delta < 0$ (dot line in Fig. 5) are oblate, the curvature of the edge sides is smaller as compared with spherical shape ($\delta = 0$). In spite of the negative δ parameter, the total shape of heavy and light fragments is, of course, prolate (quadruple moments of left and right parts of fissioning nucleus close to the scission point are positive).

Due to fluctuations, the nuclear fission does not occur with continuous stretching, as exhibited by starch syrup. Beyond the saddle and around the scission point the vibration of the length and breadth of the fissioning fragments takes place until the nucleus is split suddenly into two pieces by a strong vibration of the length ($-\delta$ direction), which reduces the density in the neck region [38]. We can conclude that the width of the peaks of the MDF is determined by such fluctuations near the scission point. Since the calculated in [10] MDF is in a good agreement with the experimental data, it supports our conclusion that the vibration of the nuclear shape is essential to describe nuclear fission correctly.

V. NUCLEAR SHAPE AT SCISSION POINT AND THE TOTAL KINETIC ENERGY

In Sec. IV, we pointed out that the nuclear shape with a negative δ , particularly around the scission point, is very important in fission dynamics. The motion of trajectories in the negative δ direction driven by the random

force leads to the splitting into fragments. The examples of nuclear shapes around the scission point are presented in Fig. 5. The shape denoted by the dot line is close to that obtained using the statistical scission model in Fig. 5 of reference [39].

The distribution of the deformation parameter δ at the scission point for the fission of ^{236}U at $E^* = 20$ MeV is shown in Fig. 6. One can see that the contribution of

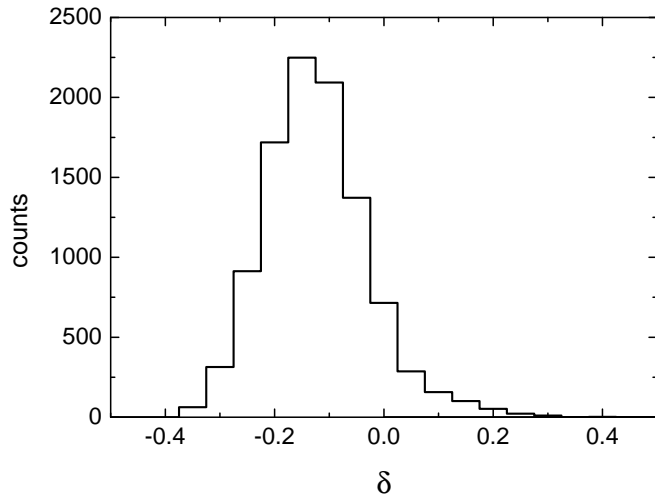


FIG. 6: The calculated distribution of fission events in the deformation parameter δ at the scission point for the fission of ^{236}U at $E^* = 20$ MeV.

fragments with negative values of δ is dominant.

To clarify the configuration at the scission point, we investigate the TKE of the fission fragments. The scission configuration is defined as the shape with neck radius equal to zero [10], and the TKE is assumed to be given by

$$TKE = V_{Coul} + E_{pre}, \quad (7)$$

where V_{Coul} and E_{pre} are the Coulomb repulsion energy of point charges of fragments and the pre-scission kinetic energy. The V_{Coul} is defined as $V_{Coul} = Z_1 Z_2 e^2 / D$, where Z_1 and Z_2 are the charges of each fragment, and D is the distance between centers of mass of left and right parts of nucleus at the scission point. We do not assume that the distance between centers of mass is that of the nascent fragments, like it is done in the statistical models in order to calculate the TKE.

The pre-scission kinetic energy E_{pre} is the kinetic energy

$$E_{kin} = \frac{1}{2} (m^{-1})_{ij} p_i p_j \quad (8)$$

calculated at the scission point. The average of E_{pre} over all fission events is equal to 7.03 MeV. So, the main contribution to the total kinetic energy comes from the Coulomb repulsion of fission fragments.

For the average value of TKE of the fission fragments $\langle TKE \rangle$ of ^{236}U at $E^* = 20$ MeV we obtained $\langle TKE \rangle = 169.5$ MeV, what is in agreement with the experimental

data (168.2 ~ 171 MeV) [40]. Because of this agreement with the experimental data for the TKE, we conclude that the configuration at the scission point is compact, such as that shown by the dot line in Fig. 5.

The TKE distribution of the fission fragments of this system is shown in Fig. 7. The distribution is approxi-

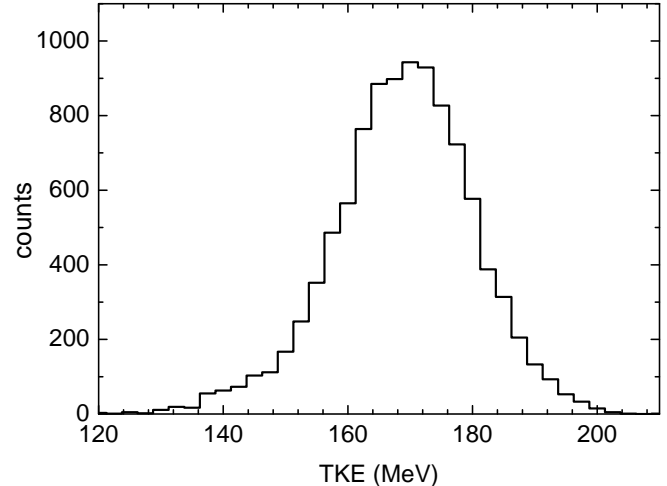


FIG. 7: The TKE distribution of the fission events of ^{236}U at $E^* = 20$ MeV.

mately Gaussian.

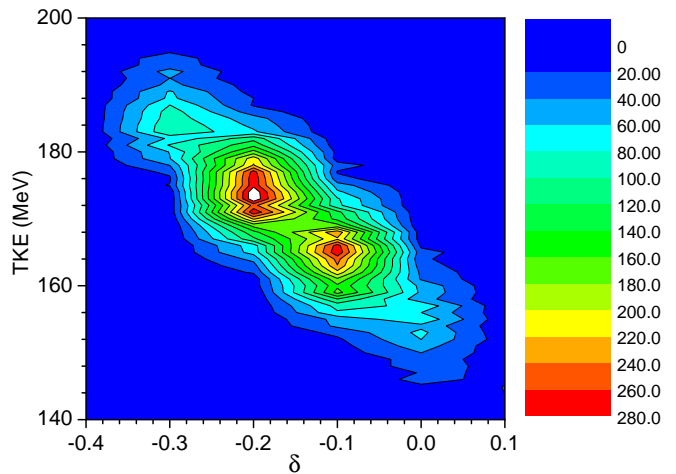


FIG. 8: The distribution of fission events of ^{236}U at $E^* = 20$ MeV in the TKE and the parameter δ .

Fig. 8 shows the distribution of fission events in the total kinetic energy and parameter δ . From this figure one can see the correlation between the TKE and the value of parameter δ at the scission line. The configuration with a negative δ corresponds to the compact shape. The TKE of such fragments is higher than that of fragments with a positive δ . The fissioning fragments with the compact configuration are dominant in this system.

VI. SUMMARY

In present paper we investigated the fission process at low excitation energy using the Langevin equations. By analyzing the trajectories calculated within our model [10], we have clarified the contributions of the mass-asymmetric fission events of ^{236}U at low excitation energy. In this way we gave an explanation for the mass-asymmetric fission of ^{236}U by the dynamical approach based on fluctuation-dissipation theorem.

The mass distribution of fission fragments of ^{236}U at $E^* = 20$ MeV is mass-asymmetric. We have found out that position of the peak is related to the position of the saddle point, which is defined mainly by the shell correction energy. In order to escape from the potential pocket around the ground state or the second minimum, almost all trajectories pass through the fission saddle point and move to the mass-asymmetric fission region. After overcoming the fission saddle points, the trajectories fluctuate frequently due to the random force in the Langevin equation and approach the scission point. The fluctuation around the scission point determines the widths of the peaks of the MDF. F.

By analyzing the fission process and investigating the shape evolution, we have found that the motion in the negative δ direction around the scission point is essential for the fission process. We stress that nuclear fission does not occur with continuous stretching, such as that observed in starch syrup. Rather, due to the shape vibration of the length and breadth of the fissioning fragments, the nucleus is suddenly split by a strong vibration in the negative δ direction. Such a mechanism in fission dynamics and the configuration with negative δ values at the scission point are supported by the fact that the calculated MDF and TKE show good agreement with the experimental data in reference [10].

In addition, we pointed out that the trajectories do not always move along the bottom of the potential energy valley owing to the random force, nor fluctuate around the trajectory without the random force (mean trajectory). Although the analysis of the fission process using the static potential energy surface gives a reasonable results in some cases, it is not enough to describe the complicated dynamics of the fission process. In this paper, we stress the importance of the dynamical treatment of the fission process.

As further study, we plan to improve the model by increasing the number of variables, namely by introducing independent deformation parameters δ_1 and δ_2 for each fragment. We have also to consider the effects of nuclear structure on the transport coefficients and the fact that Einstein relation that does not hold true at low excitation energies [33–35]. Moreover, the neutron emission from the fissioning system and from the fission fragments should be included in the model. With such improvements of the model, we aim to diminish the differences between the calculated MDF and the experimental data.

Acknowledgments

Present study is the results of ‘‘Comprehensive study of delayed-neutron yields for accurate evaluation of kinetic of high-burn up reactors’’ entrusted to Tokyo Institute of Technology by the Ministry of Education, Culture, Sports, Science and Technology of Japan (MEXT). The authors are grateful to Dr. A. Iwamoto, Prof. M. Ohta, Prof. T. Wada, Dr. K. Nishio, Dr. A.V. Karpov and Prof. V.I. Zagrebaev for their helpful suggestions and valuable discussions. Special thanks are deserved to Mr. K. Hanabusa (HPC Systems Inc.) for his support to operate the high performance computer.

Appendix

The momentum independent part $V(\rho, z)$ of the TCSM Hamiltonian is formed by the two deformed oscillator potentials joined smoothly by the fourth order polynomial in z ,

$$V(\rho, z) = \begin{cases} \frac{1}{2}m\omega_{z1}^2(z-z_1)^2 + \frac{1}{2}m\omega_{\rho1}^2\rho^2, & z \leq z_1 \\ \frac{1}{2}m\omega_{z1}^2(z-z_1)^2 f_1(z, z_1) \\ + \frac{1}{2}m\omega_{\rho1}^2\rho^2 f_2(z, z_1), & z_1 \leq z \leq 0 \\ \frac{1}{2}m\omega_{z2}^2(z-z_2)^2 f_1(z, z_2) \\ + \frac{1}{2}m\omega_{\rho2}^2\rho^2 f_2(z, z_2), & 0 \leq z \leq z_2 \\ \frac{1}{2}m\omega_{z2}^2(z-z_2)^2 + \frac{1}{2}m\omega_{\rho2}^2\rho^2, & z_2 \leq z, \end{cases} \quad (9)$$

see Fig. 9. Here m is a nucleon mass and ω_z, ω_ρ are the oscillator frequencies in z and ρ directions. The functions f_1 and f_2 are given by

$$\begin{aligned} f_1(z, z_i) &= 1 + c_i(z-z_i)/z_i + d_i(z-z_i)^2/z_i^2, \\ f_2(z, z_i) &= 1 + g_i(z-z_i)^2/z_i^2. \quad i = 1, 2. \end{aligned} \quad (10)$$

The potential $V(\rho, z)$ is characterized by 12 parameters, see (9). After imposing condition that the parts of potential are joined smoothly at $z = z_1, z = z_2$ and $z = 0$ the number of independent parameters is reduced to five: the distance $z_0 = z_2 - z_1$ between centers of oscillator potentials, the mass asymmetry α , the deformation δ_1 and δ_2 of left and right oscillator potentials and the neck parameter ϵ . The neck parameter ϵ is given by the ratio of the potential height E at $z = 0$ to the value E_0 of left and right harmonic oscillator potentials at $z = 0$ (which should be the same), see Fig 9.

All the parameters appearing in (9) are expressed in terms of these 5 deformation parameters

$$\begin{aligned} z_1 &= -z_0 \omega_{z2}/(\omega_{z1} + \omega_{z2}), \quad z_2 = z_0 \omega_{z1}/(\omega_{z1} + \omega_{z2}), \\ c_1 &= c_2 = 2 - 4\epsilon, \quad d_1 = d_2 = 1 - 3\epsilon \\ g_1 &= -\frac{\omega_{\rho1}^2 - \omega_{\rho2}^2}{\omega_{\rho1}^2} \frac{\omega_{z2}}{\omega_{z1} + \omega_{z2}}, \quad g_2 = \frac{\omega_{\rho1}^2 - \omega_{\rho2}^2}{\omega_{\rho2}^2} \frac{\omega_{z1}}{\omega_{z1} + \omega_{z2}} \end{aligned} \quad (11)$$

The ratio of oscillator frequencies ω_ρ/ω_z or the ratio of semi-axes in ρ and z directions are related to the deformation parameters δ_i ,

$$\frac{\omega_{\rho i}}{\omega_{z i}} = \frac{a_i}{b_i} = (1 - \frac{2}{3}\delta_i) / (1 + \frac{1}{3}\delta_i), \quad (12)$$

see Fig. 9. Notice that $\delta_i < 1.5$ since $a_i > 0$ and $b_i > 0$.

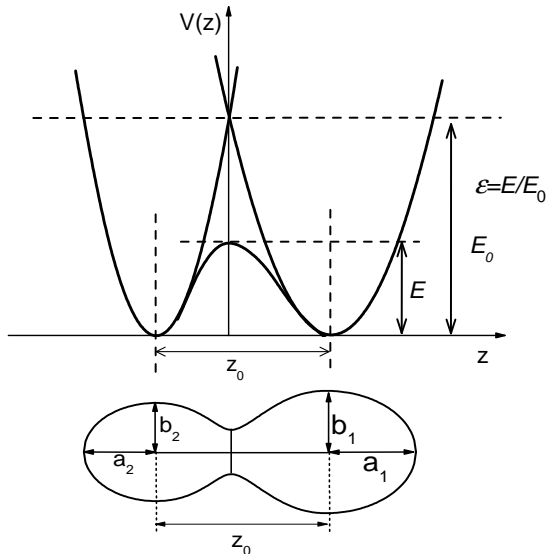


FIG. 9: The z -dependence of the potential $V(\rho, z)$ (9) (top) and the example of the equipotential surface of potential $V(\rho, z)$ (bottom). The neck parameter ϵ is defined as the ratio of the smoothed potential height E at $z = 0$ to the original one E_0 .

The ratio $\omega_{\rho 1}/\omega_{\rho 2}$ should be found numerically from the condition $(V_L - V_R)/(V_L + V_R) = \alpha$, were V_L and V_R are the volumes of left and right parts of nucleus. In TSCM parameterization the shape is divided in parts by the point $z = 0$.

The parameter ϵ is defined in the same way as in Ref. [12, 41]. With $\epsilon < 1$, the surface of two fragments shows the smooth curve at the connecting point of them. On the other hand, in the case of $\epsilon = 1$, the two fragments are connected with a sharp point like a top of cone.

We define the sharp surface shape of the fissioning nu-

clei $\rho(z)$ as that given by the equipotential surfaces of potential $V(\rho, z)$, i.e. by the equation

$$V(\rho(z), z) = V_0. \quad (13)$$

The constant V_0 in (13) is found from the requirement that the volume inside equipotential surface is equal to the volume of spherical nucleus.

The advantage of the two-center shell model parameterization is that besides the commonly used in the theory of nuclear fission degrees of freedom for the elongation, mass asymmetry and neck radius it allows the independent variation of the deformation of left and right parts of nucleus (fragments). Besides, this parameterization describes both compact shapes and separated fragments what makes it possible to describe fusion and fission processes within the same shape parameterization.

Please, note that the neck radius depends on all 5 deformation parameters. Even keeping neck parameter ϵ

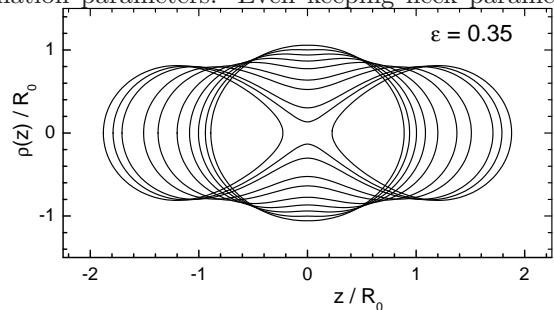


FIG. 10: The examples of shapes (13) for few values of z_0 at fixed $\alpha = 0$, $\delta_1 = \delta_2 = 0$, $\epsilon = 0.35$.

fixed one can get a full variety of fission shapes from sphere to the two separated fragments, see Fig. 10.

-
- [1] O. Hahn and F. Straßmann, *Naturwissenschaften* **27**, 11 (1939).
 - [2] L. Meitner and O.R. Frisch, *Nature (London)* **143**, 239 (1939).
 - [3] N. Bohr and J.A. Wheeler, *Phys. Rev.* **56**, 426 (1939).
 - [4] C. Schmitt, J. Bartel, K. Pomorski, and A. Surowiec, *Acta Phys. Polo. B* **34**, 1651 (2003).
 - [5] C. Schmitt, J. Bartel, A. Surowiec, and K. Pomorski, *Acta Phys. Polo. B* **34**, 2135 (2003).
 - [6] T. Asano, T. Wada, M. Ohta, T. Ichikawa, S. Yamaji, and H. Nakahara, *J. Nucl. Radiochem. Sci.* **5**, 1 (2004).
 - [7] H. Goutte, J.F. Berger, P. Casoli, and D. Gogny, *Phys. Rev. C* **71**, 024316 (2005).
 - [8] J. Randrup and P. Möller, *Phys. Rev. Lett.* **106**, 132503 (2011).
 - [9] F.A. Ivanyuk, *Phys. Procedia* **47**, 17 (2013).
 - [10] Y. Aritomo and S. Chiba, *Phys. Rev. C* **88**, 044614 (2013)
 - [11] Y. Aritomo and M. Ohta, *Nucl. Phys. A* **744**, 3 (2004).
 - [12] J. Maruhn and W. Greiner, *Z. Phys.* **251**, 431 (1972).
 - [13] K. Sato, A. Iwamoto, K. Harada, S. Yamaji, and S. Yoshida, *Z. Phys. A* **288**, 383 (1978).
 - [14] S. Yamaji, H. Hofmann and R. Samhammer, *Nucl. Phys. A* **457**, 487 (1988).
 - [15] H.J. Krappe, J.R. Nix, and A.J. Sierk, *Phys. Rev. C* **20**, 992 (1979).
 - [16] V.M. Strutinsky, *Nucl. Phys. A* **95**, 420 (1967); *A* **122**, 1 (1968).
 - [17] M. Brack, J. Damgaard, A.S. Jensen, H.C. Pauli, V.M. Strutinsky and C.Y. Wong, *Rev. Mod. Phys.* **44**, 320 (1972).
 - [18] S. Suekane, A. Iwamoto, S. Yamaji, and K. Harada, *JAERI-memo* 5918 (1974).
 - [19] A. Iwamoto, S. Yamaji, S. Suekane, and K. Harada, *Prog. Theor. Phys.* **55**, 115 (1976).
 - [20] S.G. Nilsson, C.F. Tsang, A. Sobiczewski et al, *Nucl. Phys. A* **131**, 1 (1969).

- [21] A.V. Ignatyuk, G.N. Smirenkin, and A.S. Tishin, Sov. J. Nucl. Phys. **21**, 255 (1975).
- [22] J. Toke, W.J. Swiatecki, Nucl. Phys. A **372**, 141 (1981).
- [23] A.V. Ignatyuk, K.K. Istekov, and G.N. Smirenkin, Sov. J. Nucl. Phys. **30**, 626 (1979).
- [24] A.V. Karpov, P.N. Nadtochy, E.G. Ryabov, and G.D. Adeev, J. Phys. G: Nucl. Part. Phys. **29** 2365 (2003).
- [25] K. Sato, S. Yamaji, K. Harada, and S. Yoshida, Z. Phys. A **290**, 149 (1979).
- [26] J.-J. Gaimard and K.-H. Schmidt, Nucl. Phys. A **531**, 709 (1991).
- [27] K.-H. Schmidt, H. Delagrange, J.P. Dufour, N. Carjan and A. Fleury, Z. Phys. A **308**, 215 (1982).
- [28] J. Blocki, Y. Boneh, J.R. Nix, J. Randrup, M. Robel, A.J. Sierk, and W.J. Swiatecki, Ann. Phys. **113**, 330 (1978).
- [29] J.R. Nix and A.J. Sierk, Nucl. Phys. A **428**, 161c (1984).
- [30] H. Feldmeier, Rep. Prog. Phys. **50**, 915 (1987).
- [31] T. Wada, Y. Abe and N. Carjan, Phys. Rev. Lett. **70**, 3538(1993).
- [32] K.T.R. Davies, A.J. Sierk, and J.R. Nix, Phys. Rev. C **13**, 2385 (1976).
- [33] F.A. Ivanyuk, H. Hofmann, V.V. Pashkevich, S. Yamaji, Phys. Rev. C **55**, 1730 (1997).
- [34] H. Hofmann, Phys. Rep. **284**, 137 (1997).
- [35] S. Yamaji, F.A. Ivanyuk, H. Hofmann, Nucl. Phys. A **612**, 1 (1997).
- [36] A.V. Karpov, P.N. Nadtochy, D.V. Vanin, and G.D. Adeev, Phys. Rev. C **63**, 054610 (2001).
- [37] N. Carjan, F.-J. Hamsch, F. A. Ivanyuk, P. Talou, submitted to Physics Procedia.
- [38] A. Iwamoto, and F.A. Ivanyuk, private communication.
- [39] P. Fong, Phys. Rev. **102**, 434 (1956).
- [40] R. Vandenbosh and J.R. Huizenga, *Nuclear Fission*, Academic Press, New York and London (1973).
- [41] V.I. Zagrebaev, A.V. Karpov, Y. Aritomo, M.A. Naumenko, and W. Greiner, Physics of Particles and Nuclei **38**, 469 (2007); NRV codes for driving potential, <http://nrv.jinr.ru/nrv/>.